# Design and Synthesis of Antiblinking and Antibleaching Quantum Dots in Multiple Colors via Wave Function Confinement

Hujia Cao,[†] Junliang Ma,[†] Lin Huang, Haiyan Qin,* Renyang Meng, Yang Li, and Xiaogang Peng*[ID]

Center for Chemistry of Novel & High-Performance Materials, Department of Chemistry, Zhejiang University, Hangzhou 310027, China

S *Supporting Information*

ABSTRACT: Single-molecular spectroscopy reveals that photoluminescence (PL) of a single quantum dot blinks, randomly switching between bright and dim/dark states under constant photoexcitation, and quantum dots photobleach readily. These facts cast great doubts on potential applications of these promising emitters. After ~20 years of efforts, synthesis of nonblinking quantum dots is still challenging, with nonblinking quantum dots only available in red-emitting window. Here we report synthesis of nonblinking quantum dots covering most part of the visible window using a new synthetic strategy, i.e., confining the excited-state wave functions of the core/shell quantum dots within the core quantum dot and its inner shells (≤ ~5 monolayers). For the red-emitting ones, the new synthetic strategy yields nonblinking quantum dots with small sizes (~8 nm in diameter) and improved nonblinking properties. These new nonblinking quantum dots are found to be antibleaching. Results further imply that the PL blinking and photobleaching of quantum dots are likely related to each other.
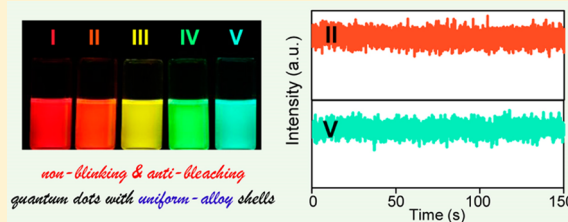
INTRODUCTION

Colloidal quantum dots are nanometer-sized fragments of the corresponding bulk crystals and synthesized in solution. The luminescence properties of quantum dots are size dependent due to quantum confinement,[1] which makes them as promising emitters for important applications, such as light-emitting-diodes,[2−4] single-biomolecular tracking,[5−7] single-photon light sources,[8,9] and so forth. Most of these applications often require continuous and stable emission yet with a relatively small sizes, usually 1−20 nm in diameter, for quantum confinement, biological permeability, and colloidal stability. However, it was reported in 1996 that the photoluminescence (PL) of single quantum dot blinks, randomly switching between bright and dim/dark states under constant photo-excitation.[10] Furthermore, single-dot measurements revealed that quantum dots photobleached readily if they were not embedded in polymer.[10−13] During the past 20 years, synthesis of nonblinking quantum dots has been an important topic in the field.[12−23] Recently, nearly nonblinking quantum dots, defined as with ≥ ~95% of time in the bright state and 5% of time in the dim/dark states in average under constant radiation,[12,13,21,24] in the red colors became available with CdSe/CdS core/shell nanocrystals.[12,13,21,24] To the best of our knowledge, nonblinking quantum dots in different colors other than red in the visible window remain unknown. Furthermore, synthesis of antibleaching quantum dots within typical size range of quantum dots has been barely explored. It should be noted that completely nonblinking CdSe/CdS core/shell nanocrystals were reported with large yet alloyed cores and extremely thick shells, so-called bulky-shell quantum dots,[25]

though these nanocrystals were likely too large to exhibit different colors through quantum confinement.

It is generally accepted that epitaxial growth of a semiconductor shell with its conduction (valence) band higher (lower) than that of the core quantum dot would enhance its photochemical and photophysical stability.[26] As a result, all synthetic efforts for nonblinking quantum dots have been focused on such type of core/shell quantum dots.[12−14,16−23] Theoretical analysis suggests that suppression of blinking might be associated with suppression of Auger effects of quantum dots.[27−29] This mechanism would in turn imply synthesis of core/shell quantum dots with two types of band structures. In the first type, the core quantum dot and its epitaxial shell forms quasi-type-II band structure, usually with the hole wave function localized in the core and electron wave function efficiently delocalized into the shell to suppress the Auger effects. The successful system of this type is the well-established CdSe/CdS core/shell quantum dots.[12,13,16−19,21,25] The second type relies on a gradient band structure of the shell, which can be synthesized by epitaxy of a gradient alloy shell onto the core quantum dot.[21,23,29,30] As both types of core/shell quantum dots require electron and/or hole wave function significantly and continuously delocalizes into the shell, the emission color of the resulting core/shell quantum dots would be limited to the long wavelength range allowed by quantum confinement, i.e., red emitters for commonly studied II−VI semiconductor nanocrystals.

It should be noted that the PL blinking of a single quantum dot under constant excitation is considered as a result of circulation from its neutral (bright) state and charged (dark/dim) state(s).[10] Though initiation of a blinking cycle is often considered as a result of Auger ionization of bi- and multiexcitons,[10,27,31−33] some reports[33−35] challenged the Auger mechanism. Our recent results identified that the charging process was linearly dependent on the excitation photon density in both single exciton—photogenerated electron—hole pair—and multiexciton regimes for CdSe/CdS core/shell quantum dots.[24] This means that Auger ionization did not play a noticeable role in initiation of blinking, which would further imply a different design principle for synthesis of nonblinking quantum dots, i.e., spatial confinement of exciton into the core and inner portion of the shells. We would anticipate that quantum dots with such spatially confined excitons should also be antibleaching. This is so because photobleaching can be considered as a photocatalytic reduction/oxidation process and surface delocalization of the photogenerated hole/electron in a quantum dot is thus necessary.

In this work, we would explore the design principle mentioned in the above paragraph. Instead of aiming to suppress Auger effects, we synthesize core/shell quantum dots with tight confinement of both electron and hole wave functions within the core and inner shells ($\leq \sim 5$ monolayers), which should presumably yield quantum dots with variable colors and small sizes ($\leq \sim 8$ nm). To realize such a structure, both conduction- and valence-band potential steps between the core and shell were chosen to be sharp and steep, opposite to the gradient potential steps achieved through those core/shell quantum dots with gradient-alloy shells.[21,23,29,30] Specifically, CdSe quantum dots were applied as the core nanocrystals except those for the blue-cyan colors with $CdSe_yS_{1−y}$ alloy cores. Uniform-alloy $Cd_xZn_{1−x}S$ was applied as the epitaxial shells with thickness in the range between 6 and 8 monolayers.

■ RESULTS AND DISCUSSION

Choice of the Core/Shell Quantum Dots with Wave Function Confinement. CdSe quantum dots are the current workhorse in the field of quantum dots, including development of core/shell ones. CdSe quantum dots are difficult to realize nonblinking core/shell ones for blue-cyan colors. Instead, we applied $CdSe_yS_{1−y}$ alloy nanocrystals as the cores (Figure 1). With CdSe (or $CdSe_yS_{1−y}$) quantum dots as the cores, common choices of the shells could be ZnS,[36] CdS,[37] and ZnSe.[38] Among them, ZnSe shells offer limited spatial confinement for the hole wave function of a CdSe core nanocrystal and was thus not considered.

Lattice mismatch between a pair of core−shell semiconductors dictates quality of the epitaxy. Spatial confinement of the exciton wave functions of a core/shell quantum dot depends on the band offsets between the core and shell semiconductors. With CdSe cores, CdSe/CdS core/shell quantum dots are the best developed system in the field.[12,13,16,17,37,39] This is so mainly because of the tolerable lattice mismatch between the core and the shells ($\sim 4\%$) and good confinement of the hole wave function (Figure 1a). However, the CdS shells provide limited spatial confinement of the electron wave function in a CdSe/CdS core/shell quantum dot.[37] Conversely, among all II−VI semiconductors, ZnS possesses the widest bandgap to offer desired spatial confinement for both electron and hole but its lattice constant differs
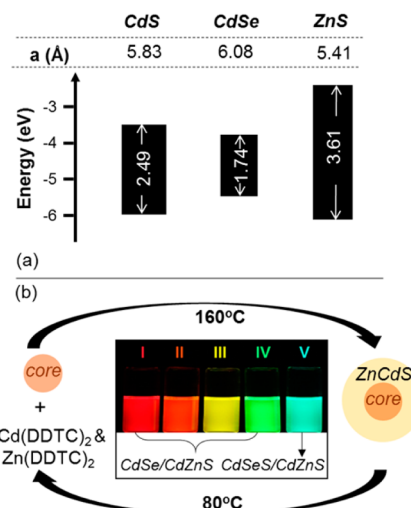

Figure 1. (a) Lattice constant (a (Å)) and energy band alignment of bulk CdS, CdSe, and ZnS in zinc-blende structure. (b) Schematic monolayer-by-monolayer epitaxy for quantum dots with the uniform-alloy shells with different emission colors using cadmium diethyldithiocarbamate ($Cd(DDTC)_2$) and zinc diethyldithiocarbamate ($Zn(DDTC)_2$) as the mixed single precursors. Samples I and II with 6-monolayer uniform-alloy shells, Samples III−V with 8-monolayer uniform-alloy shells. These sample codes might be applied repeatedly in this report.

from that of CdSe greatly (Figure 1a). Literature reports revealed that the large lattice mismatch ($>11\%$) between CdSe and ZnS makes high-quality epitaxy with necessary shell thickness challenging.[36,40] We anticipate that tight spatial confinement for both electron and hole wave functions and excellent epitaxy might be simultaneously achievable with uniform-alloy shells of a CdS−ZnS mixture ($Cd_{1−x}Zn_xS$, $x =$ constant).

Synthesis of Core/Shell Quantum Dots with the Uniform-Alloy Shells. Synthesis of alloy quantum dots was explored more than 10 years ago.[41−43] Specifically for the $Cd_{1−x}Zn_xS$ shells, Xie et al. previously demonstrated that gradient composition change from pure CdS to pure ZnS for the shells of CdSe core nanocrystals would greatly relax the strain energy and realize core/shell quantum dots with high PL quantum yield (QY).[43]

The key synthetic challenge for realizing tunable yet controlled spatial confinement of wave functions is to perform epitaxy with uniform and targeted alloy composition throughout the shells. Previous report[44] revealed that, by enabling epitaxy at a relatively low temperature (<200 °C), one could prevent interdiffusion between Zn and Cd ions within the lattices of II−VI semiconductors. Highly reactive single-source precursors, namely cadmium diethyldithiocarbamate (Cd-$(DDTC)_2$) and zinc diethyldithiocarbamate ($Zn(DDTC)_2$), were proven to respectively enable epitaxy of the CdS[45] and ZnS[44] shells at a temperature significantly below 200 °C. To suppress self-nucleation of the shell materials, we adopted a thermocycling technique[44] by addition of the precursors at 80 °C and subsequent epitaxial growth at 160 °C for growth of each monolayer of the targeted shells (Figure 1b) (see details in the Experimental Section). As references, CdSe quantum dots with either pure CdS or gradient-alloy ($Cd_{1−x}Zn_xS$, x increased gradually from the first monolayer to the outmost monolayer) epitaxial shells were synthesized. For simplicity, the uniform-
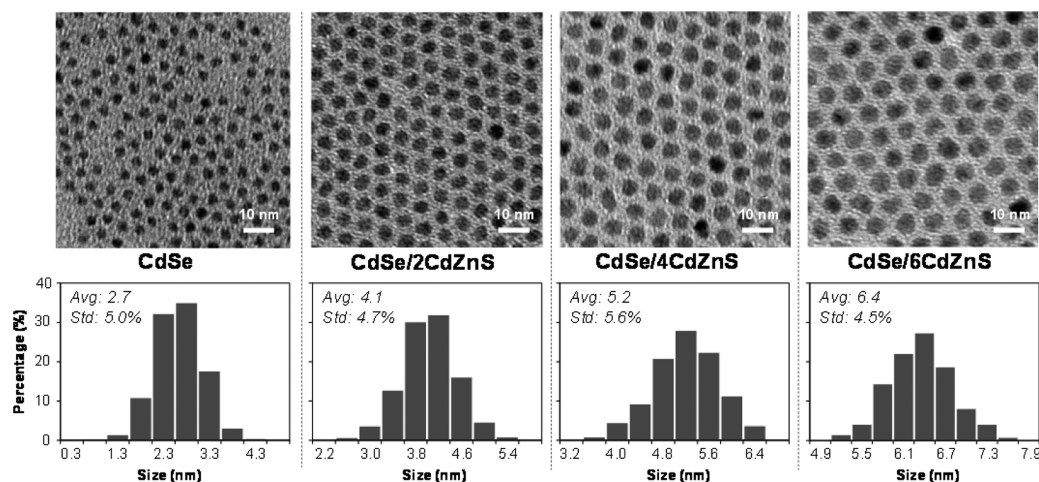
Figure 2. Evolution of size and size distribution of nanocrystals during epitaxial growth of Sample II.
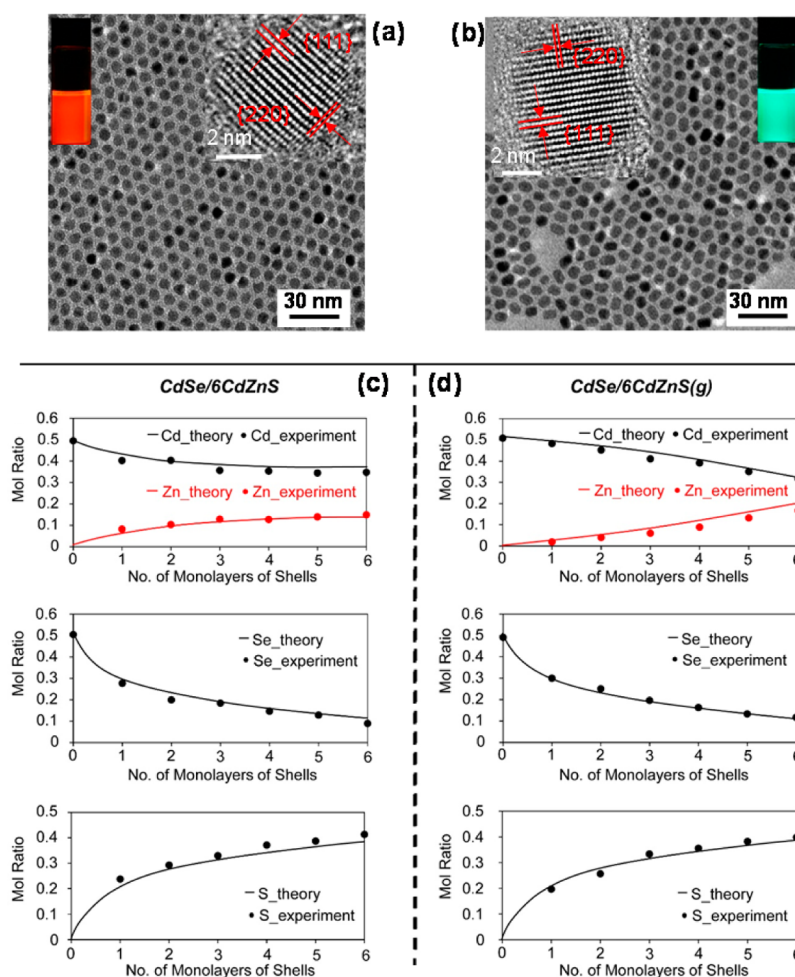

Figure 3. Representative TEM and HRTEM (insets) of Sample II (a) and V (b). (c) Experimental (dots) and targeted (solid lines) inorganic elemental compositions (top, Cd and Zn; middle, Se; bottom, S) of CdSe (2.6 nm) based core/shell QDs with 0−6 monolayers of the uniform-alloy ($Cd_{0.65}Zn_{0.35}S$) shells (c) and gradient-alloy shells (d). For the gradient-alloy shells, the ratios between $Zn(DDTC)_2$ and $Cd(DDTC)_2$ precursors added into the reaction solution increased gradually from 0.05 (1st), 0.15 (2nd), 0.24 (3rd), 0.33 (4th), 0.42 (5th), to 0.50 (6th).

alloy and gradient-alloy shells may be named as "CdZnS" and "CdZnS(g)" shells, respectively.

Transmission electron microscopy (TEM) confirmed that, upon epitaxial growth of the uniform-alloy shells, the size increased in good accordance with the intended number of monolayers (Figure 2). The resulting core/shell nanocrystals remained nearly spherical in shape along the epitaxial growth (Figure 2, top). The size distribution of the core/shell quantum dots with uniform-alloy shells retained the narrow size distribution of the core dots. Consistent with TEM results in

Figure 2, the absorption and PL spectra of the core/shell quantum dots (Figure S1) remained similar sharpness of the initial core ones though epitaxial growth of the uniform-alloy shells somewhat shifted the PL peaks (Figure S1, Table S1, and more discussions below). As expected for the growth of wide bandgap shells, there was significant increase of relative absorbance at high-energy side in the absorption spectra of the final core/shell quantum dots with the uniform-alloy shells (Figure S1).

Similar level of control on size/shape and size/shape distribution of the core/shell quantum dots with the uniform-alloy shells was reproducible for those with CdSe core quantum dots. In comparison, the core/shell dots with $CdSe_yS_{1-y}$ alloy cores were less controllable, with their shape being often slightly elongated (compare Figures 3a with b). Nevertheless, high-resolution TEM and X-ray powder diffraction (XRD) confirmed that all core/shell quantum dots with the uniform-alloy shells were single-crystalline in zinc-blende structure (Figure 3a, b insets and Figure S2). The PL peak position and quantum yield of the core/shell quantum dots with the alloy cores exhibited a larger degree of variation. For instance, the PL quantum yield of all core/shell quantum dots was 90 ± 5% but it was toward the low end in the range for those with the alloy cores (Table S1). All these results implied that there are significant room for improvement for the alloy/alloy core/shell quantum dots.

Energy-dispersive X-ray spectroscopy (EDX) was applied to confirm the monolayer-by-monolayer elemental composition of both uniform-alloy and gradient-alloy shells (Figure 3c and d).

Upon epitaxy of the uniform-alloy shells with appropriate Cd:Zn ratios for different core quantum dots, it was possible to completely stop the red shift of the PL peaks of the quantum dots with the shell thickness between 6 and 8 monolayers (Figure 4a). This indicated delocalization of the exciton wave
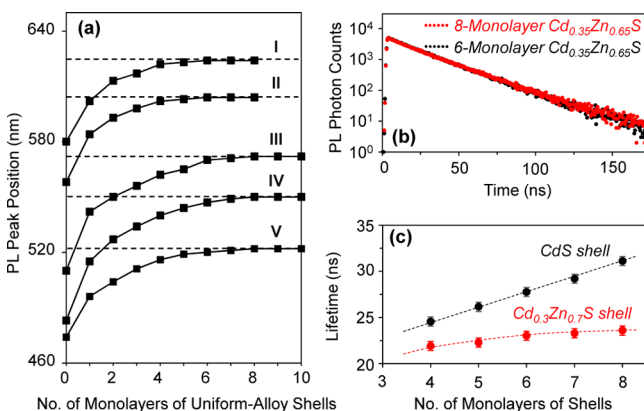
The spatial wave function confinement of the quantum dots with the uniform-alloy shells became further evident by comparing the same batch of core quantum dots with three types of shells (Figure S3, Supporting Information). Starting from CdSe core quantum dots with their PL peak at 558 nm, we found that 6 monolayers of the uniform-alloy ($Cd_{0.65}Zn_{0.35}S$) shells yielded orange-emitting (~604 nm) quantum dots with complete wave function confinement (Figure 4a). Conversely, pure CdS shells with the same shell thickness shifted the PL peak to ~616 nm (Figure S3a, Supporting Information), and the red-shift would continue for at least 16 monolayers of the pure CdS shells.[46] Degree of spatial wave function confinement by the gradient-alloy shells were between that of the CdS and the uniform-alloy shells (Figure S3a, Supporting Information).

While the PL peak position of the quantum dots with 6−8 monolayers of the uniform-alloy shells did not show red-shift, the PL decay dynamics of the corresponding quantum dots also held steady (see Figurs 4b and c for examples). In comparison, the PL decay lifetime increased significantly and continuously for the quantum dots with all thickness of the CdS shells (Figures 4c and S3b). In principle, PL decay dynamics of a quantum dot should be dominated by the spatial overlapping of the photogenerated electron/hole wave functions and accessible defect states. The unaltered PL decay dynamics (Figure 4b and c) suggested that both photogenerated electron and hole wave functions were localized within the core and inner uniform-alloy shells, given the substantially different effective mass of the electron and hole of CdSe.[1] Furthermore, 6 monolayers of the uniform-alloy shells seemed to be sufficient to isolate the excitons from the defects at inorganic−organic interface and further growth to 8 monolayers did not create additional defects within the core and inner shells.

Results revealed that, the higher the emission energy of the core (or resulting core/shell) quantum dots was, the more delocalization into the shell would be. This required increase of the Zn/Cd ratio in the uniform-alloy shells for the quantum dots with high emission energy to suppress the wave function delocalization with a limited shell thickness. Excess Zn in the uniform-alloy shells for a given core, such as $Cd_{0.44}Zn_{0.56}S$ shell for 3 nm CdSe core dots (Figure S4, Supporting Information), would result in core/shell quantum dots with irregular shape and poor size distribution, indicating poor-quality epitaxy. Fortunately, tolerance of the Zn/Cd ratio in the uniform-alloy shells increased as the size (or emission wavelength) of the core quantum dots decreased. Existence of an up limit of the Zn/Cd ratio in the uniform-alloy shells limited the emission colors to green, yellow, orange, and red (emission wavelength >540 nm) for CdSe-based core/shell quantum dots with complete spatial wave function confinement (Figures 1b and 4a). Quantum dots with the uniform-alloy shells in the blue/cyan window (~480−530 nm) were realized by using alloyed $CdSe_yS_{1-y}$ core quantum dots (Figures 1b and 4a).

Ensemble and Single-Dot Optical Properties of Quantum Dots with Uniform-Alloy Shells. With well-controlled epitaxy, quantum dots with the uniform-alloy shells possessed PL quantum yield are 90 ± 5% (Table S1, Supporting Information) and nearly monoexponential PL decay dynamics (Figures 4b and 5, left panel). The maximum counts for each transient PL measurement in Figure 5 (left) were 5,000. Each curve was fitted by a single-exponential function for the entire range, and the monoexponential lifetime (τ) and the corresponding goodness-of-fit (χ_R^2) are given for

Figure 4. (a) Evolution of PL peak position upon epitaxy of the uniform-alloy shells. (b) PL decay dynamics of quantum dots with 6- and 8-monolayer uniform-alloy shells. (c) Shell-thickness dependent PL decay lifetime of 3 nm CdSe quantum dots coated with different shells. The error bars come from the measurement errors of the instrument.

functions was spatially confined within a certain thickness of the uniform-alloy shells, i.e., within ~5 monolayers. To achieve similar level of wave function confinement in Figure 4a, the zinc content with the alloy shells needed to be increased as the PL peak of the core quantum dots shifted to blue (see detail below).
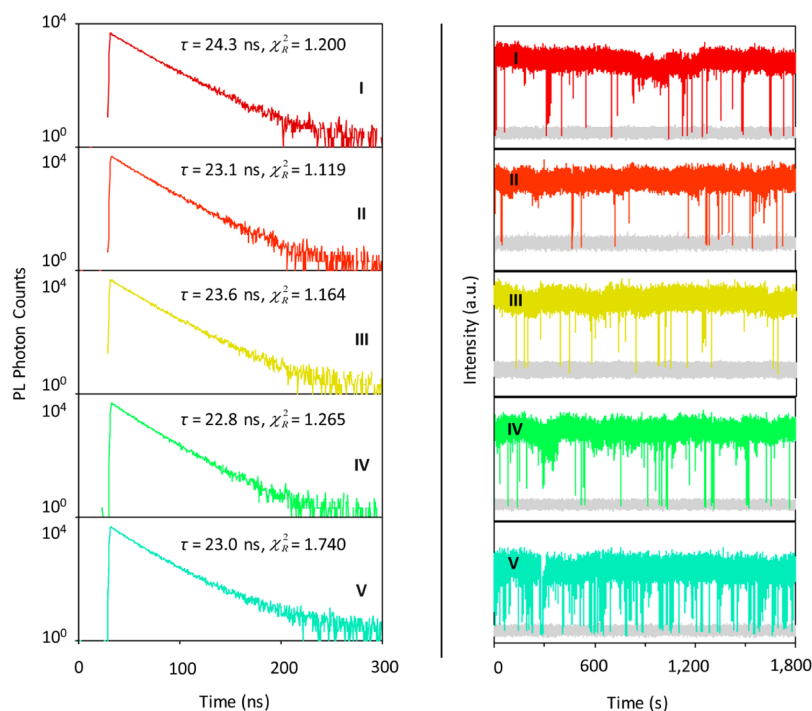
Figure 5. Left: Ensemble PL decay dynamics of five representative samples. Right: Representative PL intensity trajectories in 1800 s for five representative samples. All curves in this figure are color-coded with their PL colors.

each curve in the plot. Evidently, all samples with CdSe cores and uniform-alloy shells were sufficiently monoexponential (χ_R^2 = 1.000−1.300). Sample V with CdSe$_y$S$_{1−y}$ cores and uniform-alloy shells was slightly deviated from monoexponential with χ_R^2 = 1.740. This was found to be consistent with the slightly less control on the shape of the core/shell quantum dots with CdSe$_y$S$_{1−y}$ cores (Figure 3b).

Single-dot optical properties of core/shell quantum dots were studied using home-built setups described previously.[13] The PL intensity trajectories with an extended time window (1800 s) are shown in Figure 5 (right panel) for the quantum dots in five representative colors, namely cyan, green, yellow, orange, and red, revealing their nearly nonblinking behavior. Within typical 100−500 s time windows used in literature, a good portion of the quantum dots with the uniform-alloy shells might not blink at all (Figure S5, Supporting Information).

Statistically, the on-fraction averaged for 50−70 quantum dots for each sample (Figures 6a and S6) was >95%. PL spectra of a single quantum dot for all colors resembled those of the corresponding solutions but with narrower peak width (Figure 6b), indicating rooms for further synthetic improvement of these new quantum dots. Consistent with the TEM (Figure 3) and ensemble PL decay dynamics (Figure 5, left panel), the PL peak of the single dot with CdSe$_y$S$_{1−y}$ cores was comparatively broader than that for the others with CdSe cores. The $g^2(0)$ values in the second-order photon correlation measurements for all samples were usually smaller than 0.1, indicating the emission of single dots (Figure 6c).[47]

Rate of initiation of PL blinking—from bright to dim/dark state—could be calculated[24] (Figure S7, Supporting Information). Complementary to the average on-fraction, the rates give tendency of initiation of a blinking cycle. In comparison to the well-established CdSe/CdS core/shell quantum dots with similar emission color, the rates of initiation of PL blinking for the quantum dots with the uniform-alloy shells reduced by

∼10−20 times under the same excitation conditions (Figure S7, Supporting Information). All quantum dots with CdSe core and the uniform-alloy shells emitting green, yellow, organ, and red colors showed similar resistance to the PL blinking (Figures 5 (right panel) and 6a). Comparatively, the cyan-blue emitting quantum dots with CdSe$_y$S$_{1−y}$ core and Cd$_{1−x}$Zn$_x$S uniform-alloy shells were less resistant (Figure 5, right panel), but their rates of initiation of PL blinking were still ∼2 times lower than that of the nonblinking CdSe/CdS core/shell quantum dots only available in the red window (Figure S7, Supporting Information). Quantum dots with either pure CdS shells or gradient-alloy shells synthesized in this work—both with limited available colors as nonblinking ones—were nearly nonblinking under typical measurement conditions, but they would become problematic without polymer protection (see below).

Single-Dot Spectroscopy of the Quantum Dots without Polymer Protection. if the quantum dots with 6 monolayers of the pure CdS shells were directly exposed in air on a glass substrate without polymer protection, they went through photobleaching rapidly (Figure 7a, right column) upon continuous laser irradiation (445 nm, power density of 135 W/cm^2). For the quantum dots with the gradient-alloy shells (Figure 7a, middle column), photobleaching was retarded noticeably with the same average photons absorbed[48] by each dot (445 nm, power density of 320 W/cm^2). The quantum dots with the same CdSe core but the uniform-alloy shells showed impressive resistance to photobleaching, i.e., practically no sign of photobleaching in air (Figure 7a, left column).

Quantitatively, photobleaching of all three types of core/shell quantum dots obeyed single-exponential kinetics (Figure 7b). The time constant for photobleaching of the quantum dots with the uniform-alloyed shells was too large to be determined accurately (∼5000 min or greater). In comparison, the time constant of the first-order kinetics of photobleaching for the
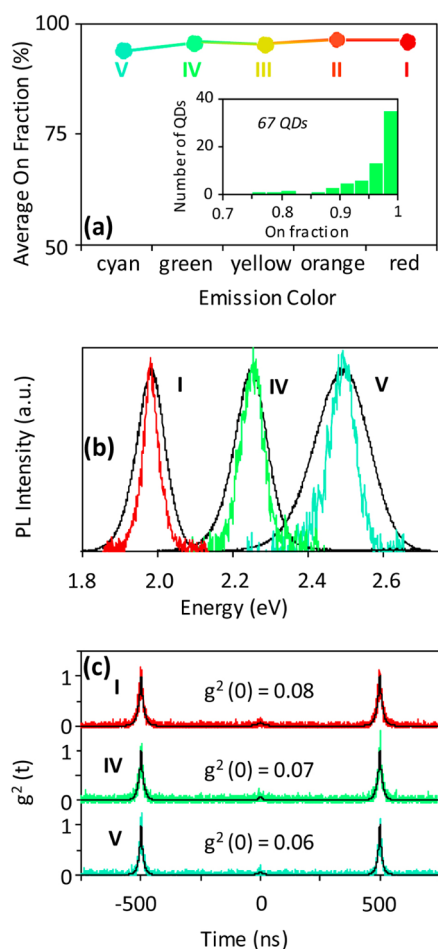
Figure 6. (a) Averaged on-fraction statistics for 50−70 quantum dots for each sample in a time window of 150 s. Inset: On-fraction distribution of the green-emitting quantum dots (Sample IV). (b) Normalized PL spectra of single (color coded) and ensemble (black) quantum dots. (c) Representative photon antibunching curves of single red-, green-, and cyan-emitting quantum dots.

quantum dots with the CdS and gradient-alloy shells was 6 and 15 min, respectively. These values were ∼3 orders of magnitude smaller than that of the quantum dots with the uniform-alloy shells.

The outstanding antibleaching properties of the quantum dots with 6−8-monolayer uniform-alloy shells enabled their single-molecular spectroscopy studies in air. Though the experimental conditions were too challenging for the quantum dots with either pure CdS or gradient-alloy shells, the quantum dots with the uniform-alloy shells demonstrated nearly nonblinking behavior in air. For the example shown in Figure 7c, the average on-fraction for 50 orange-emitting quantum dots with the uniform-alloy shells was still >95% with majority of single quantum dots with 98−100% on-fraction. In air, rate of initiation of PL blinking (bright to dim/dark) for the quantum dots with the gradient-alloy shells, only counting the quantum dots without bleaching, was about ∼4 times higher than that for the quantum dots with the uniform-alloy shells (Figure S8, Supporting Information). Consistent with their slightly worse antiblinking feature (Figure 5, right panel), the cyan-emitting quantum dots with $CdSe_yS_{1-y}$ cores were found to be less resistant to photobleaching. This might be because the cyan-emitting quantum dots were less developed, indicated

by their relatively broad size/shape distribution (Figure 3) and slight less control on PL decay dynamics (Figure 5, left panel). Active research is under way to further develop the cyan- and blue-emitting quantum dots with uniform-alloy shells.

Antiblinking and antibleaching quantum dots are of critical importance for most of their promising applications as emissive materials. For instance, quantum-dots light-emitting-diodes in red colors with nearly ideal performance were developed[4] after nearly nonblinking and highly efficient CdSe/CdS core/shell quantum dots with good stability, with 10 monolayers of CdS shells, became available.[13] The nonblinking quantum dots with small physical sizes demonstrated above (≤8 nm in diameter, Table S1) should be of interest for biomedical labeling. For biomedical applications, it would require ligand exchange of the quantum dots from the original hydrophobic ligands to hydrophilic ones. The original ligands of all three types of quantum dots in Figure 7 were successfully replaced with mercaptopropionic acid ligands in methanol (see Experimental Section). After the ligand exchange, quantum dots with the uniform-alloy shells almost retained their PL quantum yield and nonblinking characteristics (Figure S9, Supporting Information). The ligand exchange impacted the optical properties of quantum dots with the pure CdS shells seriously and worsened the PL properties of the quantum dots with gradient-alloy shells to a certain extent (Figure S9, Supporting Information).

Results above indicate that delocalization of excitons onto the nanocrystal-ligands interface is the key for suppressing both blinking and bleaching. Given the stability order of antiblinking of three types of core/shell quantum dots, Auger effects are unlikely playing a decisive role in initiation of PL blinking. In addition, the order of lattice stress within three types of core/shell quantum dots is evidently opposite to that of antiblinking and antibleaching. Thus, lattice strain within the core/shell quantum dots is not the key parameter for suppression of blinking and bleaching as long as it does not create noticeable structural disorder during epitaxy.

■ CONCLUSION

In summary, high-quality epitaxy of $Cd_xZn_{1-x}S$ uniform-alloy shells onto CdSe and $CdSe_yS_{1-y}$ core quantum dots can offer complete spatial confinement of the exciton wave functions within the core and inner portion of the shells, which rendered the quantum dots to be antiblinking and antibleaching with relatively small sizes (≤ ∼8 nm). Results suggested that PL blinking and photobleaching correlated each other positively. This correlation seemed reasonable by considering PL blinking and photobleaching of quantum dots respectively as reversible and irreversible photoionization processes. The spatial wave function confinement extended the emission window of nonblinking quantum dots beyond red colors to cover most visible colors. These high PL quantum yield, small-sized, antiblinking, and antibleaching quantum dots with continuously tunable emission colors should greatly promote quantum dots for realization of their applications as emissive materials. Furthermore, the synthetic scheme presented here should be applicable for other combinations of the core and shell semiconductors to achieve programmable and well-controlled spatial distribution of the wave functions of quantum dots for other purposes, such as photovoltaic devices[49,50] and photo-catalysts.[51,52]
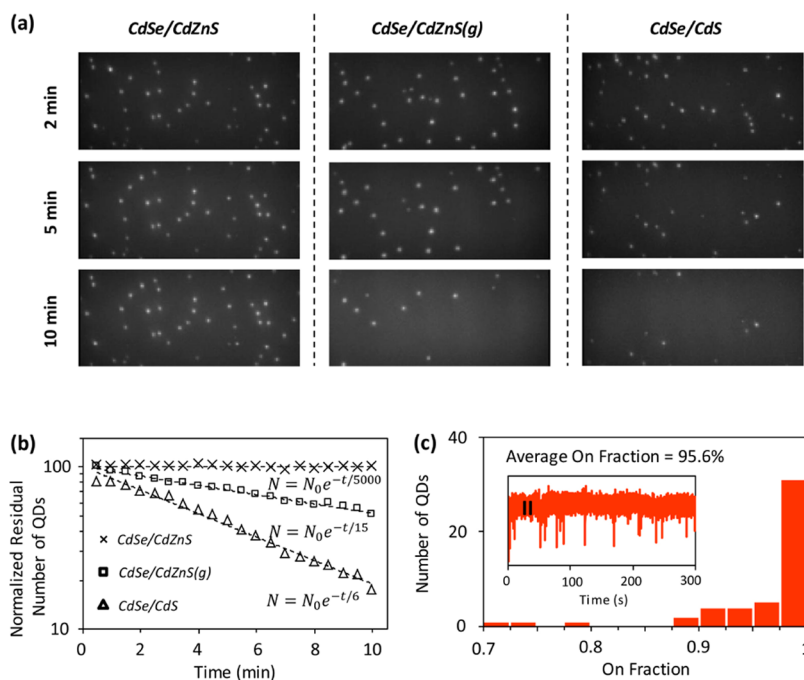
Figure 7. (a) PL images of three types of core/shell quantum dots with the same core and shell thickness under constant irradiation of 445 nm laser in air. (b) Single-exponential kinetics of photobleaching for three types of core/shell quantum dots. The fitting functions are provided in the plot (dashed lines) with N and t being the normalized number of residual quantum dots and the corresponding time, respectively. (c) On-fraction distribution of 50 orange-emitting quantum dots with the uniform-alloy shells taken in air. Inset: Representative PL intensity trajectory taken in air.

■ EXPERIMENTAL SECTION

Chemicals. 1-Octadecene (ODE, 90%), dodecane (99%), octylamine (99%), stearic acid (HSt, 90+%), selenium powder (Se, 200 mesh, 99.999%), and tetramethylammonium hydroxide (TMAH, 98%) were purchased from Alfa-Aesar. Sulfur powder (S, 99.98%), oleylamine (NH$_2$Ol, 70%), mercaptopropionic acid (MPA), and poly(methyl methacrylate) (PMMA) were obtained from Aldrich. Tributylphosphine (TBP) was provided by Shanghai Titan Chem. Cadmium acetate dihydrate (Cd(Ac)$_2$·2H$_2$O, 98.5%) was purchased from Shanghai Tingxin Reagents. Zinc acetate dihydrate (Zn(Ac)$_2$·2H$_2$O, 98.5%) was purchased from Shanghai Meixing Chemical Corporation. Sodium diethyldithiocarbamate trihydrate (NaDDTC·3H$_2$O, 99%) was provided by Aladdin Reagents. All organic solvents were purchased from Sinopharm Reagents. All chemicals above were used directly without any purification.

Synthesis of Cadmium Stearate (Cd(St)$_2$). HSt (20 mmol) and equal-moles of tetramethylammonium hydroxide were dissolved in 250 mL of methanol. Into this solution, Cd(Ac)$_2$·2H$_2$O (10 mmol) dissolved in 50 mL of methanol was added dropwise under vigorous stirring. Stirring continued for another 20 min after the dropping was completed. White Cd(St)$_2$ precipitate was collected through filtration and washed three times with methanol. The product was ready for further use after 24 h drying under vacuum.

Synthesis of Cadmium Diethyldithiocarbamate (Cd(DDTC)$_2$) and Zinc Diethyldithiocarbamate (Zn(DDTC)$_2$). Cd(Ac)$_2$·2H$_2$O (10 mmol) was dissolved into 200 mL of distilled water in a 400 mL beaker. NaDDTC·3H$_2$O (20 mmol) dissolved in 60 mL of distilled water was added dropwise under vigorous stirring. Another 20 min of stirring was provided for completion of the Cd(DDTC)$_2$ precipitation. White Cd(DDTC)$_2$ precipitate was collected through filtration and washed three times with distilled water. The product was dried under vacuum for 24 h for future use. Synthesis of Zn(DDTC)$_2$ was the same except replacing Cd(Ac)$_2$·2H$_2$O with equal-mole of Zn(Ac)$_2$·2H$_2$O. For epitaxial growth of the shells, the shell precursor solutions were prepared with a given molar ratio of Cd(DDTC)$_2$ and Zn(DDTC) in dodecane-amine (3 to 1 ratio) solution (0.1 mmol/mL in total).

Synthesis of CdSe and CdSe$_y$S$_{1-y}$ Core QDs. Synthesis of CdSe core QDs followed a procedure using "selenium suspension in ODE"

(Se-SUS).[46] For the CdSe$_y$S$_{1-y}$ core QDs, the synthetic procedure was altered by replacing Se-SUS with Se&S-SUS. Se&S-SUS was prepared by dispersing Se powder (0.0237 g, 0.30 mmol) and S powder (0.0096 g, 0.30 mmol) in ODE (3 mL) by sonication for 5 min. In a typical synthesis, Cd(St)$_2$ (0.068 g, 0.1 mmol) and ODE (3 mL) were loaded into a 25 mL three-neck flask. After bubbling with argon for 10 min, the mixture was heated to 250 °C. Se&S-SUS (0.4 mL) was injected swiftly into the reaction flask at 250 °C. After growth for 10 min, the reaction mixture was allowed to cool to 50 °C, and then an in situ purification procedure described below was conducted. To obtain different size QDs, multiple doses of Se&S-SUS were dropped into the reaction solution at 250 °C.

Synthesis of CdSe/CdZnS and CdSeS/CdZnS Core/Shell Quantum Dots. The synthetic procedure was modified from a previous report developed for synthesis of CdSe/CdS core/shell quantum dots.[13] In a typical synthesis, dodecane (1.19 mL), oleylamine (3.81 mL), and 1 mL of purified core quantum dot solution (containing ∼3 × 10^{-7} mol of nanocrystals) were added to a three-neck flask under argon flow, and then heated to 80 °C. For accurately controlling the ratio of Zn to Cd in the shell, a precursor stock solution with the same Cd(DDTC)$_2$ to Zn(DDTC)$_2$ molar ratio was applied for the growth of every monolayer for a given synthesis. For each growth cycle, addition of the precursor solutions was at 80 °C and growth of the CdZnS shells was at 160 °C for 20 min. The Zn percentages in the shells for Samples I−V in the main text were 25%, 30%, 30%, 35%, and 45%, respectively. For the control CdSe/CdZnS(g) core/shell quantum dots with the gradient-alloy shells, the Cd(DDTC)$_2$ to Zn(DDTC)$_2$ ratio in the precursor solutions for each monolayer was altered to reflect the final gradient Cd/Zn ratio in the shells. Other than this, the entire synthetic procedure was the same as that applied for the quantum dots with the uniform-alloy shells.

In Situ Purification. In situ purification was conducted to purify the core QDs. At 50 °C, TBP (0.2 mL), octylamine (0.2 mL), hexane (4 mL), and methanol (8 mL) were added into the reaction solution and stirred for 2.5 min. After turning off the stirring, the colorless methanol layer was separated from the ODE−hexane layer and removed by syringe. This purification procedure was conducted for four times, but TBP and octylamine were only added for the first and

third time. The hexane and methanol left in the ODE layer were removed by argon bubbling at about 70 °C.

Ligand Exchange. Each ligand exchange reaction for either of three types of QDs was carried out in a sealed 5 mL chromatographic bottle. Mercaptopropionic acid (100 μL) was basified to pH of ∼10 using tetramethylamonium hydroxide in 2 mL of methanol. The original solution of a given type of the core/shell QDs (200 μL) was precipitated with 300 μL of anhydrous methanol and 150 μL of oleylamine. The wet precipitate was then resuspended in 100 μL of chloroform. Subsequently, the QDs solution was injected into the mecaptopropoinic acid solution to form a cloudy suspension. After stirring for ∼1 h at 60 °C, an optically clear solution was obtained, indicating the surface ligands were switched from hydrophobic to hydrophilic ones.

Ensemble Optical Measurements. UV−vis spectra were taken on Analytik Jena S600 UV−visible spectrophotometer. Photoluminescence spectra were recorded on Edinburgh Instrument FLS920. The absolute PL QY was measured using an Ocean Optics FOIS-1 integrating sphere coupled with a QE65000 spectrometer. Measurements for gradient-diluted nanocrystal solutions were performed for each sample at room temperature. PL decay curves were measured on a time-correlated single-photon counting (TCSPC) spectrofluorometer (FLS920, Edinburgh Instrument, UK) at room temperature. The nanocrystal samples were diluted in hexane solution and excited by a 405 nm picosecond laser diode with a 2 MHz repetition rate. The peak photon counts were set at 5000 for all measurements. The PL lifetime τ was obtained by fitting the decay curve by a single-exponential decay function and χ_R^2 was the goodness-of-fit.

Transmission Electron Microscopy (TEM) and High Resolution TEM (HRTEM). TEM images were taken on a Hitachi 7700 transmission electron microscope with an acceleration voltage of 80 kV using copper grids (400-mesh) coated with pure carbon support film. HRTEM images were taken on a JEOL JEM-2100 microscope with an acceleration voltage of 200 kV using copper grids coated with ultrathin carbon film. The hexane solution containing nanocrystals were deposited onto the carbon film on copper grids.

Energy-Dispersive X-ray Spectroscopy (EDX). EDX was investigated using a FEI SIRION-100 scanning electron microscope equipped with a field emission gun and operated at 25 kV. The chloroform solution containing nanocrystals after purification was dropped onto copper sheets with conducting adhesive.

X-ray Powder Diffraction (XRD). XRD measurements were carried on a Rigaku Ultimate-IV X-ray diffractometer operated at 40 kV/30 mA with Cu Kα line (λ = 1.5418 Å). Nanocrystal powder samples were placed onto glass substrates after purification by the standard precipitation procedure with hexanes as the solvent and acetone as the precipitation reagent.

Single Quantum Dots Optical Measurements. For single-dot experiments, the procedure and home-built setups were reported previously.[13] A brief description is as follows. Diluted quantum dot solution in toluene with 3% PMMA by weight was spun casted on a clean glass coverslip. All measurements were carried out by an epi-illumination fluorescence microscope body (Olympus IX 83) with a 60× oil immersion microscope objective (Olympus, numerical aperture = 1.49). All optical measurements were performed at room temperature. All data analysis was conducted by homemade programs. For the blinking measurements, a 445 nm continuous-wave laser (A.L.S. GmbH, PiL044X) was used as the default excitation light source but a 405 nm laser was used for the cyan-emitting quantum dots. Using suitable dichroic beam splitters and long-pass filters (Semrock), the photoluminescence signals of single-quantum dots were collected and recorded by an EMCCD camera (Andor, iXon Ultra 897) or a single photon counting modules (PicoQuant, τ-SPAD, 350 ps resolution). For single-quantum dot PL blinking measurements, the integration time was 30 ms for each data point. For antibunching measurements, a 445 nm pulsed laser (A.L.S. GmbH, PiL044X) was used as the default excitation light source except for the cyan-emitting quantum dots (a 375 nm laser). Measurements were performed with a Hanbury-Brown and Twiss setup comprised of a 50/

50 fiber optic couplers (Thorlabs, FC632-50B-FC), two single photon counting modules (PicoQuant, τ-SPAD, 350 ps resolution) and a time-tagged, time-resolved (TTTR) mode of a TCSPC module (PicoQuant, PicoHarp 300). The photon arrival time was recorded with a resolution of 512 ps for TTTR mode.

Photobleaching Measurements. For the photobleaching experiments, QDs in a diluted solution in toluene were directly spun casted on a clean glass coverslip. All measurements were carried out by the epi-illumination fluorescence microscope system mentioned above. A 445 nm continuous-wave laser (PicoQuant) was used as the excitation light source. To maintain the same average number of photons absorbed by each dot in a given time period, the laser power density was 135 W/cm^2 in the case of CdSe/CdS QDs and 320 W/cm^2 in the case of alloy shells QDs. The QDs with either type of alloy shells were synthesized from the same CdSe core QDs and the overall Cd/Zn ratio in the gradient-alloy shells was the same as the fixed Cd/Zn ratio in the uniform-alloy shells. After recording a 10 min image sequence via EMCCD in 30 ms bin, images were stacked through intensity maximum algorithm in every 30 s. Therewith, the number of residual QDs of each newly binned image was counted for antibleaching analysis. This algorithm would avoid miscounting caused by the blinking, especially for the QDs with either CdS or gradient-alloy shells.

Estimation of the Photons Absorbed Per Lifetime Cycle ⟨N⟩. Calculation of absorption cross-section for uniform-alloy shells ($Cd_{1-x}Zn_xS$, x = constant) onto CdSe (or $CdSe_yS_{1-y}$) core QDs was referred to ref 45. The number of photons absorbed per lifetime ⟨N⟩ can be estimated as

$$\langle N \rangle = \frac{C_{abs} P \tau}{E(\lambda)}$$

Here C_{abs} is the calculated absorption cross section of uniform-alloy shells ($Cd_{1-x}Zn_xS$, x = constant) onto CdSe (or $CdSe_yS_{1-y}$) core QDs. C_{abs} values at each wavelength for the QDs were all corrected by the absorption spectra according to C_{abs} at 320 nm. C_{abs} at 320 nm was calculated from the bulk semiconductors. P is the excitation power density. $E(\lambda)$ is the energy for a photon with the excitation wavelength of λ. τ is the lifetime of the QDs derived from the ensemble PL decay lifetime measurements.

■ ASSOCIATED CONTENT

Ⓢ Supporting Information

The Supporting Information is available free of charge on the ACS Publications website at DOI: 10.1021/jacs.6b10102.

> Dimensional data; absorption, steady-state and transient PL spectra; schematic diagram of wave functions; XRD and TEM data; PL intensity trajectories and on-fraction statistics; calculation of charging rates (PDF)

■ AUTHOR INFORMATION

Corresponding Authors
*hattieqin@zju.edu.cn
*xpeng@zju.edu.cn
ORCID Ⓘ
Xiaogang Peng: 0000-0002-5606-8472
Author Contributions
[†]H.C. and J.M. contributed equally to this work.
Notes
The authors declare no competing financial interest.

■ ACKNOWLEDGMENTS

■ REFERENCES

(1) Brus, L. E. *J. Chem. Phys.* **1984**, *80*, 4403.

(2) Colvin, V. L.; Schlamp, M. C.; Alivisatos, A. P. *Nature* **1994**, *370*, 354.

(3) Coe, S.; Woo, W. K.; Bawendi, M.; Bulovic, V. *Nature* **2002**, *420*, 800.

(4) Dai, X.; Zhang, Z.; Jin, Y.; Niu, Y.; Cao, H.; Liang, X.; Chen, L.; Wang, J.; Peng, X. *Nature* **2014**, *515*, 96.

(5) Dahan, M.; Levi, S.; Luccardini, C.; Rostaing, P.; Riveau, B.; Triller, A. *Science* **2003**, *302*, 442.

(6) Lidke, D. S.; Nagy, P.; Heintzmann, R.; Arndt-Jovin, D. J.; Post, J. N.; Grecco, H. E.; Jares-Erijman, E. A.; Jovin, T. M. *Nat. Biotechnol.* **2004**, *22*, 198.

(7) Welsher, K.; Yang, H. *Nat. Nanotechnol.* **2014**, *9*, 198.

(8) Michler, P.; Kiraz, A.; Becher, C.; Schoenfeld, W. V.; Petroff, P. M.; Zhang, L. D.; Hu, E.; Imamoglu, A. *Science* **2000**, *290*, 2282.

(9) Lounis, B.; Moerner, W. E. *Nature* **2000**, *407*, 491.

(10) Nirmal, M.; Dabbousi, B. O.; Bawendi, M. G.; Macklin, J. J.; Trautman, J. K.; Harris, T. D.; Brus, L. E. *Nature* **1996**, *383*, 802.

(11) Schlegel, G.; Bohnenberger, J.; Potapova, I.; Mews, A. *Phys. Rev. Lett.* **2002**, *88*, 137401.

(12) Chen, O.; Zhao, J.; Chauhan, V. P.; Cui, J.; Wong, C.; Harris, D. K.; Wei, H.; Han, H. S.; Fukumura, D.; Jain, R. K.; Bawendi, M. G. *Nat. Mater.* **2013**, *12*, 445.

(13) Qin, H.; Niu, Y.; Meng, R.; Lin, X.; Lai, R.; Fang, W.; Peng, X. *J. Am. Chem. Soc.* **2014**, *136*, 179.

(14) Hohng, S.; Ha, T. *J. Am. Chem. Soc.* **2004**, *126*, 1324.

(15) He, H.; Qian, H. F.; Dong, C. Q.; Wang, K. L.; Ren, J. C. *Angew. Chem., Int. Ed.* **2006**, *45*, 7588.

(16) Mahler, B.; Spinicelli, P.; Buil, S.; Quelin, X.; Hermier, J. P.; Dubertret, B. *Nat. Mater.* **2008**, *7*, 659.

(17) Chen, Y.; Vela, J.; Htoon, H.; Casson, J. L.; Werder, D. J.; Bussian, D. A.; Klimov, V. I.; Hollingsworth, J. A. *J. Am. Chem. Soc.* **2008**, *130*, 5026.

(18) Greytak, A. B.; Allen, P. M.; Liu, W. H.; Zhao, J.; Young, E. R.; Popovic, Z.; Walker, B. J.; Nocera, D. G.; Bawendi, M. G. *Chem. Sci.* **2012**, *3*, 2028.

(19) Ghosh, Y.; Mangum, B. D.; Casson, J. L.; Williams, D. J.; Htoon, H.; Hollingsworth, J. A. *J. Am. Chem. Soc.* **2012**, *134*, 9634.

(20) Pisanello, F.; Lemenager, G.; Martiradonna, L.; Carbone, L.; Vezzoli, S.; Desfonds, P.; Cozzoli, P. D.; Hermier, J. P.; Giacobino, E.; Cingolani, R.; De Vittorio, M.; Bramati, A. *Adv. Mater.* **2013**, *25*, 1974.

(21) Park, Y. S.; Bae, W. K.; Padilha, L. A.; Pietryga, J. M.; Klimov, V. I. *Nano Lett.* **2014**, *14*, 396.

(22) Ji, B. T.; Giovanelli, E.; Habert, B.; Spinicelli, P.; Nasilowski, M.; Xu, X. Z.; Lequeux, N.; Hugonin, J. P.; Marquier, F.; Greffet, J. J.; Dubertret, B. *Nat. Nanotechnol.* **2015**, *10*, 170.

(23) Lane, L. A.; Smith, A. M.; Lian, T. Q.; Nie, S. M. *J. Phys. Chem. B* **2014**, *118*, 14140.

(24) Meng, R.; Qin, H.; Niu, Y.; Fang, W.; Yang, S.; Lin, X.; Cao, H.; Ma, J.; Lin, W.; Tong, L.; Peng, X. Submitted.

(25) Nasilowski, M.; Spinicelli, P.; Patriarche, G.; Dubertret, B. *Nano Lett.* **2015**, *15*, 3953.

(26) Peng, X. G. *Nano Res.* **2009**, *2*, 425.

(27) Efros, A. L.; Rosen, M. *Phys. Rev. Lett.* **1997**, *78*, 1110.

(28) Wang, L. W.; Califano, M.; Zunger, A.; Franceschetti, A. *Phys. Rev. Lett.* **2003**, *91*, 056404.

(29) Cragg, G. E.; Efros, A. L. *Nano Lett.* **2010**, *10*, 313.

(30) Bae, W. K.; Padilha, L. A.; Park, Y. S.; McDaniel, H.; Robel, I.; Pietryga, J. M.; Klimov, V. I. *ACS Nano* **2013**, *7*, 3411.

(31) Banin, U.; Bruchez, M.; Alivisatos, A. P.; Ha, T.; Weiss, S.; Chemla, D. S. *J. Chem. Phys.* **1999**, *110*, 1195.

(32) Peterson, J. J.; Nesbitt, D. J. *Nano Lett.* **2009**, *9*, 338.

(33) Galland, C.; Ghosh, Y.; Steinbruck, A.; Hollingsworth, J. A.; Htoon, H.; Klimov, V. I. *Nat. Commun.* **2012**, *3*, 908.

(34) Rosen, S.; Schwartz, O.; Oron, D. *Phys. Rev. Lett.* **2010**, *104*, 157404.

(35) Zhao, J.; Nair, G.; Fisher, B. R.; Bawendi, M. G. *Phys. Rev. Lett.* **2010**, *104*, 157403.

(36) Hines, M. A.; Guyot-Sionnest, P. *J. Phys. Chem.* **1996**, *100*, 468.

(37) Peng, X.; Schlamp, M. C.; Kadavanich, A. V.; Alivisatos, A. P. *J. Am. Chem. Soc.* **1997**, *119*, 7019.

(38) Reiss, P.; Bleuse, J.; Pron, A. *Nano Lett.* **2002**, *2*, 781.

(39) Li, J. J.; Wang, Y. A.; Guo, W. Z.; Keay, J. C.; Mishima, T. D.; Johnson, M. B.; Peng, X. G. *J. Am. Chem. Soc.* **2003**, *125*, 12567.

(40) Dabbousi, B. O.; RodriguezViejo, J.; Mikulec, F. V.; Heine, J. R.; Mattoussi, H.; Ober, R.; Jensen, K. F.; Bawendi, M. G. *J. Phys. Chem. B* **1997**, *101*, 9463.

(41) Zhong, X. H.; Han, M. Y.; Dong, Z. L.; White, T. J.; Knoll, W. *J. Am. Chem. Soc.* **2003**, *125*, 8589.

(42) Bailey, R. E.; Nie, S. M. *J. Am. Chem. Soc.* **2003**, *125*, 7100.

(43) Xie, R. G.; Kolb, U.; Li, J. X.; Basche, T.; Mews, A. *J. Am. Chem. Soc.* **2005**, *127*, 7480.

(44) Chen, D. A.; Zhao, F.; Qi, H.; Rutherford, M.; Peng, X. G. *Chem. Mater.* **2010**, *22*, 1437.

(45) Nan, W.; Niu, Y.; Qin, H.; Cui, F.; Yang, Y.; Lai, R.; Lin, W.; Peng, X. *J. Am. Chem. Soc.* **2012**, *134*, 19685.

(46) Niu, Y.; Pu, C. D.; Lai, R. C.; Meng, R. Y.; Lin, W. Z.; Qin, H. Y.; Peng, X. G. *Nano Res.* **2016**, DOI: 10.1007/s12274-016-1287-3.

(47) Michler, P.; Imamoglu, A.; Mason, M. D.; Carson, P. J.; Strouse, G. F.; Buratto, S. K. *Nature* **2000**, *406*, 968.

(48) Leatherdale, C. A.; Woo, W. K.; Mikulec, F. V.; Bawendi, M. G. *J. Phys. Chem. B* **2002**, *106*, 7619.

(49) Greenham, N. C.; Peng, X.; Alivisatos, A. P. *Phys. Rev. B: Condens. Matter Mater. Phys.* **1996**, *54*, 17628.

(50) McDonald, S. A.; Konstantatos, G.; Zhang, S. G.; Cyr, P. W.; Klem, E. J. D.; Levina, L.; Sargent, E. H. *Nat. Mater.* **2005**, *4*, 138.

(51) Zhu, H. M.; Song, N. H.; Lv, H. J.; Hill, C. L.; Lian, T. Q. *J. Am. Chem. Soc.* **2012**, *134*, 11701.

(52) Tarafder, K.; Surendranath, Y.; Olshansky, J. H.; Alivisatos, A. P.; Wang, L. W. *J. Am. Chem. Soc.* **2014**, *136*, 5121.